8-1-2012

Measurement of the Oxidation State of Mitochondrial Cytochrome c from the Neocortex of the Mammalian Brain

Y. Sakata
Dartmouth College

M. Abajian
Dartmouth College

M. O. Ripple
Dartmouth College

R. Springett
Dartmouth College

Biomedical Optics EXPRESS

Measurement of the oxidation state of mitochondrial cytochrome c from the neocortex of the mammalian brain

Y. Sakata, M. Abajian, M. O. Ripple, and R. Springett*

Department of Radiology, The Geisel School of Medicine at Dartmouth, Hanover, NH 03755, USA
**RSpringett@Dartmouth.edu*

Abstract: Diffuse optical remission spectra from the mammalian neocortex at visible wavelengths contain spectral features originating from the mitochondria. A new algorithm is presented, based on analytically relating the first differential of the attenuation spectrum to the first differential of the chromophore spectra, that can separate and calculate the oxidation state of cytochrome c as well as the absolute concentration and saturation of hemoglobin. The algorithm is validated in phantoms and then tested on the neocortex of the rat during an anoxic challenge. Implementation of the algorithm will provide detailed information of mitochondrial oxygenation and mitochondrial function in physiological studies of the mammalian brain.

OCIS codes: (170.0170) Medical optics and biotechnology; (170.1470) Blood or tissue constituent monitoring.

References and links

1. C. H. Snyder, E. B. Gutierrez-Cirlos, and B. L. Trumpower, "Evidence for a concerted mechanism of ubiquinol oxidation by the cytochrome bc1 complex," J. Biol. Chem. **275**(18), 13535–13541 (2000).
2. P. R. Rich, I. C. West, and P. Mitchell, "The location of CuA in mammalian cytochrome c oxidase," FEBS Lett. **233**(1), 25–30 (1988).
3. C. Hunte, H. Palsdottir, and B. L. Trumpower, "Protonmotive pathways and mechanisms in the cytochrome bc1 complex," FEBS Lett. **545**(1), 39–46 (2003).
4. B. Chance and G. R. Williams, "The respiratory chain and oxidative phosphorylation," Adv. Enzymol. Relat. Subj. Biochem. **17**, 65–134 (1956).
5. J. E. Morgan and M. Wikström, "Steady-state redox behavior of cytochrome c, cytochrome a, and CuA of cytochrome c oxidase in intact rat liver mitochondria," Biochemistry **30**(4), 948–958 (1991).
6. J. G. Lindsay, P. L. Dutton, and D. F. Wilson, "Energy-dependent effects on the oxidation-reduction midpoint potentials of the b and c cytochromes in phosphorylating submitochondrial particles from pigeon heart," Biochemistry **11**(10), 1937–1943 (1972).
7. V. S. Hollis, M. Palacios-Callender, R. J. Springett, D. T. Delpy, and S. Moncada, "Monitoring cytochrome redox changes in the mitochondria of intact cells using multi-wavelength visible light spectroscopy," Biochim. Biophys. Acta **1607**(2-3), 191–202 (2003).
8. F. G. Hempel, F. F. Jöbsis, J. L. LaManna, M. R. Rosenthal, and H. A. Saltzman, "Oxidation of cerebral cytochrome aa3 by oxygen plus carbon dioxide at hyperbaric pressures," J. Appl. Physiol. **43**(5), 873–879 (1977).
9. F. F. Jöbsis, J. H. Keizer, J. C. LaManna, and M. Rosenthal, "Reflectance spectrophotometry of cytochrome aa3 *in vivo*," J. Appl. Physiol. **43**(5), 858–872 (1977).
10. N. R. Kreisman, T. J. Sick, J. C. LaManna, and M. Rosenthal, "Local tissue oxygen tension-cytochrome a,a3 redox relationships in rat cerebral cortex *in vivo*," Brain Res. **218**(1-2), 161–174 (1981).
11. A. E. Arai, C. E. Kasserra, P. R. Territo, A. H. Gandjbakhche, and R. S. Balaban, "Myocardial oxygenation *in vivo*: optical spectroscopy of cytoplasmic myoglobin and mitochondrial cytochromes," Am. J. Physiol. **277**(2 Pt 2), H683–H697 (1999).
12. J. Mayhew, Y. Zheng, Y. Hou, B. Vuksanovic, J. Berwick, S. Askew, and P. Coffey, "Spectroscopic analysis of changes in remitted illumination: the response to increased neural activity in brain," Neuroimage **10**(3), 304–326 (1999).
13. D. Malonek and A. Grinvald, "Interactions between electrical activity and cortical microcirculation revealed by imaging spectroscopy: implications for functional brain mapping," Science **272**(5261), 551–554 (1996).
14. S. M. Narayan, E. M. Santori, A. J. Blood, J. S. Burton, and A. W. Toga, "Imaging optical reflectance in rodent barrel and forelimb sensory cortex," Neuroimage **1**(3), 181–190 (1994).

#169970 - $15.00 USD Received 6 Jun 2012; revised 19 Jul 2012; accepted 21 Jul 2012; published 25 Jul 2012

15. D. Malonek, U. Dirnagl, U. Lindauer, K. Yamada, I. Kanno, and A. Grinvald, "Vascular imprints of neuronal activity: relationships between the dynamics of cortical blood flow, oxygenation, and volume changes following sensory stimulation," Proc. Natl. Acad. Sci. U.S.A. **94**(26), 14826–14831 (1997).
16. M. Jones, J. Berwick, and J. Mayhew, "Changes in blood flow, oxygenation, and volume following extended stimulation of rodent barrel cortex," Neuroimage **15**(3), 474–487 (2002).
17. U. Lindauer, J. Gethmann, M. Kühl, M. Kohl-Bareis, and U. Dirnagl, "Neuronal activity-induced changes of local cerebral microvascular blood oxygenation in the rat: effect of systemic hyperoxia or hypoxia," Brain Res. **975**(1-2), 135–140 (2003).
18. M. Kohl, U. Lindauer, G. Royl, M. Kuhl, L. Gold, A. Villringer, and U. Dirnagl, "Physical model for the spectroscopic analysis of cortical intrinsic optical signals," Phys. Med. Biol. **45**(12), 3749–3764 (2000).
19. R. B. Buxton, "The elusive initial dip," Neuroimage **13**(6), 953–958 (2001).
20. M. Jones, J. Berwick, D. Johnston, and J. Mayhew, "Concurrent optical imaging spectroscopy and laser-Doppler flowmetry: the relationship between blood flow, oxygenation, and volume in rodent barrel cortex," Neuroimage **13**(6), 1002–1015 (2001).
21. J. Mayhew, D. Johnston, J. Martindale, M. Jones, J. Berwick, and Y. Zheng, "Increased oxygen consumption following activation of brain: theoretical footnotes using spectroscopic data from barrel cortex," Neuroimage **13**(6), 975–987 (2001).
22. U. Lindauer, G. Royl, C. Leithner, M. Kühl, L. Gold, J. Gethmann, M. Kohl-Bareis, A. Villringer, and U. Dirnagl, "No evidence for early decrease in blood oxygenation in rat whisker cortex in response to functional activation," Neuroimage **13**(6), 988–1001 (2001).
23. I. Vanzetta and A. Grinvald, "Evidence and lack of evidence for the initial dip in the anesthetized rat: implications for human functional brain imaging," Neuroimage **13**(6), 959–967 (2001).
24. E. M. Hillman, D. A. Boas, A. M. Dale, and A. K. Dunn, "Laminar optical tomography: demonstration of millimeter-scale depth-resolved imaging in turbid media," Opt. Lett. **29**(14), 1650–1652 (2004).
25. M. Paoli, J. Marles-Wright, and A. Smith, "Structure-function relationships in heme-proteins," DNA Cell Biol. **21**(4), 271–280 (2002).
26. C. Cooper, M. Sharpe, C. Elwell, R. Springett, J. Penrice, L. Tyszczuk, P. Amess, J. Wyatt, V. Quaresima, and D. Delpy, "The cytochrome oxidase redox state *in vivo*," Adv. Exp. Med. Biol. **428**, 449–456 (1997).
27. R. Springett, J. Newman, M. Cope, and D. T. Delpy, "Oxygen dependency and precision of cytochrome oxidase signal from full spectral NIRS of the piglet brain," Am. J. Physiol. Heart Circ. Physiol. **279**(5), H2202–H2209 (2000).
28. G. L. Liao and G. Palmer, "The reduced minus oxidized difference spectra of cytochromes a and a3," Biochim. Biophys. Acta **1274**(3), 109–111 (1996).
29. C. R. Simpson, M. Kohl, M. Essenpreis, and M. Cope, "Near-infrared optical properties of *ex vivo* human skin and subcutaneous tissues measured using the Monte Carlo inversion technique," Phys. Med. Biol. **43**(9), 2465–2478 (1998).
30. L. G. Henyey and J. L. Greenstein, "Diffuse radiation in the galaxy," Astrophys. J. **93**, 70–83 (1941).
31. S. R. Arridge, M. Cope, and D. T. Delpy, "The theoretical basis for the determination of optical pathlengths in tissue: temporal and frequency analysis," Phys. Med. Biol. **37**(7), 1531–1560 (1992).
32. H. J. van Staveren, C. J. M. Moes, J. van Marie, S. A. Prahl, and M. J. C. van Gemert, "Light scattering in Intralipid-10% in the wavelength range of 400-1100 nm," Appl. Opt. **30**(31), 4507–4514 (1991).
33. D. F. Wilson, M. Erecińska, C. Drown, and I. A. Silver, "Effect of oxygen tension on cellular energetics," Am. J. Physiol. **233**(5), C135–C140 (1977).
34. G. De Visscher, R. Springett, D. T. Delpy, J. Van Reempts, M. Borgers, and K. van Rossem, "Nitric oxide does not inhibit cerebral cytochrome oxidase *in vivo* or in the reactive hyperemic phase after brief anoxia in the adult rat," J. Cereb. Blood Flow Metab. **22**(5), 515–519 (2002).
35. J. C. Finlay and T. H. Foster, "Effect of pigment packaging on diffuse reflectance spectroscopy of samples containing red blood cells," Opt. Lett. **29**(9), 965–967 (2004).
36. R. Springett, M. Wylezinska, E. B. Cady, M. Cope, and D. T. Delpy, "Oxygen dependency of cerebral oxidative phosphorylation in newborn piglets," J. Cereb. Blood Flow Metab. **20**(2), 280–289 (2000).
37. D. R. Green and G. Kroemer, "The pathophysiology of mitochondrial cell death," Science **305**(5684), 626–629 (2004).
38. M. O. Ripple, M. Abajian, and R. Springett, "Cytochrome c is rapidly reduced in the cytosol after mitochondrial outer membrane permeabilization," Apoptosis **15**(5), 563–573 (2010).

1. Introduction

The optical attenuation spectrum of the mammalian brain is dominated by the absorption of hemoglobin at visible wavelengths and the mitochondrial cytochromes, which are heme containing proteins of the electron transport chain, only make a minor contribution. The absorption band of the hemes change depending on whether the heme is reduced (carrying an electron) or oxidized (not carrying an electron) and this property has been used repeatedly to probe function of the isolated enzymes [1–3] and mitochondrial preparations [4–6] using two-wavelength difference spectrophotometry, and we have developed a full-spectral system to calculate the oxidation changes of all the mitochondrial hemes from cells in suspension [7]. In the late 1970s and early 1980s, the two-wavelength technique was used to measure oxidation

#169970 - $15.00 USD Received 6 Jun 2012; revised 19 Jul 2012; accepted 21 Jul 2012; published 25 Jul 2012

changes of cytochrome oxidase from the exposed mammalian cortex [8–10] but there was considerable skepticism that this method could accurately separate the cytochrome signal from the much greater hemoglobin signals and this technique has not been pursued into the present day. Few attempts have been made to measure the cytochromes with modern multi-wavelength visible spectroscopy systems probably because of their controversial history, problems with crosstalk and the difficulty in validating the signal. Where they have been measured [11,12], they have not been quantified [11] or interpreted [11,12]. Improvements in spectroscopic detection and our understanding of the light transport through tissue now warrant a reexamination of the problem as these mitochondrial signals are sensitive to both mitochondrial function and mitochondrial oxygenation and thus have the potential to provide valuable physiological information on the energy metabolism of the brain.

Current optical imaging systems either image the brain illuminated with several wavelengths of monochromatic light [13,14] or use a spectrograph with a CCD detector to measure full spectra along a line across the cortex [15–17]. Each of these techniques only measure changes in hemoglobin concentration from the change in attenuation spectrum by applying a modified Beer-Lambert law. They all require a model to calculate the differential pathlength, which must be based on estimations of the underlying hemoglobin concentration and saturation as well as tissue scattering coefficient. Furthermore, the wavelength dependence of the differential pathlength distorts the attenuation spectrum compared to the chromophore extinction spectra leading to crosstalk between the hemoglobin signals [18]. This has led to controversy with regard to the "initial dip" in functional activation studies [19–23], the presence or absence of which depends on small changes in deoxyhemoglobin (Hb) in the presence of large changes in oxyhemoglobin (HbO_2). A recent innovation is laminar optical tomography (LOT) [24] in which the image of a laser spot and the image of multiple detector fibers is scanned across the cortex with mirrors mounted on galvanometers. The detector fibers are mounted at differing separations from the laser spot so that they sample different depths into the tissue and it is possible to reconstruct a 3-dimensional image of the cortex. However, even this technique uses an estimate of the baseline hemoglobin concentration to reconstruct tomographic images of hemoglobin concentration.

The mitochondrial electron transport chain contains 7 hemes embedded in 4 proteins: complex II contains b_{560}, the bc_1 complex contains b_L, b_H and c_1 (hence its name), Cyt*c* contains a c-type heme and CytOx contains heme *a* and a_3. The hemes are classed as either a, b or c-type depending on modifications to the porphyrin ring [25] and the modification, combined with the protein environment, confers each of the 7 heme centers a distinct absorption spectrum. Typically, the reduced heme has a strong and sharp absorption band whereas the oxidized heme has a broader and weaker absorption spectrum.

The mitochondrial cytochromes are present in the brain at much lower concentrations than hemoglobin and the absorption spectrum of the hemes is weaker than hemoglobin in part because each molecule of hemoglobin contains four hemes. Together, this makes the cytochrome signals highly susceptible to crosstalk from the hemoglobin. The cytochromes with the highest concentration in the brain, and so most amenable to separation from the hemoglobin signals, are cytochrome c (Cyt*c*) and cytochrome oxidase (CytOx). Cyt*c* is a 12.5KDa protein with an absorption band at 550nm which diffuses in the intermembrane space and transfers electrons from the bc_1 complex to CytOx. CytOx contains four redox centers. The Cu_A center is the electron acceptor from Cyt*c*. From there, electrons are passed to the heme *a* center and then to the binuclear center consisting of heme a_3 and Cu_B where oxygen is reduced to water. Oxidized Cu_A has an absorption band at 830nm and the oxidation changes have been measured with near infrared spectroscopy [26,27]. Cyt*c* and Cu_A have similar midpoint potentials, are on the same side of the inner mitochondrial membrane and are expected to be in redox equilibrium and so provide essentially the same information. Both the heme *a* and heme a_3 centers have absorption bands at 605nm which cannot be resolved spectroscopically. However the mixed signal, often referred to as $Cytaa_3$, is dominated by the heme *a* center as it has the stronger absorption band [28].

#169970 - $15.00 USD Received 6 Jun 2012; revised 19 Jul 2012; accepted 21 Jul 2012; published 25 Jul 2012

The goal of this paper is to introduce and validate a new algorithm based on the first differential of the attenuation spectrum combined with a Monte Carlo simulation of the light transport through tissue to calculate the concentration of reduced Cyt*c*, as well as the absolute hemoglobin concentration and saturation, from the attenuation spectrum from the exposed cerebral cortex of small animals. To this end, studies were performed in phantoms where the concentration of Hb, HbO_2 and reduced Cyt*c* could be varied independently and, for the first time, from the cerebral cortex of rats during a brief anoxic challenge.

2. Methods

2.1. Instrumentation

An optode probe was developed that could be placed against the thinned skull of a rat that consisted of two 400μm fibers with a numerical aperture of 0.37 separated by 1mm housed in a 6.35mm diameter black-acetal rod. The probe was also used for the phantom studies. The source optode was coupled to a stabilized tungsten halogen lamp filtered with a KG2 heat absorbing filter to remove the infrared and a BG38 colored glass filter to shape the incident light spectrum to match the hemoglobin absorption spectrum. Output power at the sample was ≈160μW. Light from the detector fiber was F#-matched onto the slits of an F4.0, 0.3m spectrograph (Triax 320, JY Horiba, Edison, NJ,) equipped with a 600g/mm grating blazed at 500nm. Complete spectra between 508 and 640nm were collected on a 1024 × 128 pixel back-thinned CCD (charge coupled device) detector with 26 × 26μm pixels cooled to 210 Kelvin (DV401BV, Andor Technology, Hartford, CT). The spectrograph was wavelength calibrated daily against the green and yellow-doublet mercury lines. The pixel bandpass was ≈0.13nm and the slits set to 200μm to give a spectral resolution of ≈1nm. Spectra were intensity calibrated against a polytetrafluoroethylene (PTFE or Teflon®) phantom. Spectra were collected contiguously at 50Hz and every 25 attenuation spectra were averaged to give a temporal resolution of 0.5seconds.

2.2. Algorithms

The attenuation, *A*, of light through tissue is defined as

$$A(\lambda) = -\mathrm{Ln}\left(I_D(\lambda)/I_S(\lambda)\right) \tag{1}$$

where λ is wavelength, $I_D(\lambda)$ is the detected light intensity, and $I_S(\lambda)$ is the source light intensity. Assuming a given anisotropy factor, the attenuation can be modeled as a function of tissue absorption coefficient (μ_a) and reduced scattering coefficient (μ_s) which are both dependent on wavelength. The absorption is the sum of the absorption from the tissue chromophores weighted by their concentration, e.g.,

$$\mu_a(\lambda) = \sum_k C_k \varepsilon_k(\lambda) \tag{2}$$

where C_k is the concentration of the *k*th chromophore, $\varepsilon_k(\lambda)$ is the specific absorption spectrum of the *k*th chromophore in natural log units and the sum is over all the chromophores. Most present day spectroscopy systems measure the change in the attenuation and relate it to the change in chromophore concentration and change in scattering through:

$$\Delta A = \frac{\partial A}{\partial \mu_a}\Delta\mu_a + \frac{\partial A}{\partial \mu_s}\Delta\mu_s = \rho\Delta\mu_a + \sigma\Delta\mu_s \tag{3}$$

where ρ has units of length and is called the differential pathlength by analogy with the Beer-Lambert law and σ has units of length and is referred to here as the differential scatterlength as it has units of length and is the scattering equivalent of the differential pathlength. Both terms are wavelength dependent. Usually it is assumed that the scattering coefficient does not

#169970 - $15.00 USD Received 6 Jun 2012; revised 19 Jul 2012; accepted 21 Jul 2012; published 25 Jul 2012

change so that $\Delta\mu_s$ is zero and then the change in attenuation is related to the change in chromophore concentrations by

$$\Delta A(\lambda) = \rho(\lambda)\sum_k \Delta C_k \varepsilon_k(\lambda) \tag{4}$$

This is the formal derivation of the modified Beer-Lambert law. The change in chromophore concentration can be calculated from the change in attenuation spectrum measured at multiple wavelengths using a classical least-squares algorithm if the chromophore extinction spectra are known.

Attempts to measure the absolute concentration of hemoglobin directly from the attenuation spectrum using a Monte Carlo simulation to model the relationship between attenuation and absorption coefficient have been largely unsuccessful [18]. The relationship between attenuation and chromophore concentration is highly non-linear and dependent on boundary conditions. We have taken a different approach to calculating absolute chromophore concentrations from the attenuation spectra. If the attenuation spectrum is differentiated with respect to wavelength then, because attenuation is a function of μ_a and μ_s, the first differential is given by

$$\frac{dA(\lambda)}{d\lambda} = A'(\lambda) = \frac{\partial A}{\partial \mu_a}\frac{d\mu_a}{d\lambda} + \frac{\partial A}{\partial \mu_s}\frac{d\mu_s}{d\lambda} \tag{5}$$

The first term on the right is just the product of the differential pathlength and the first differential of the specific extinction chromophores weighted by their concentration, whereas the second term is the product of the differential scatterlength and the first differential of the scattering coefficient with respect to wavelength. Thus Eq. (5) reduces to

$$A'(\lambda) = \rho(\lambda)\sum_k C_k \varepsilon_k'(\lambda) + \sigma(\lambda)\varepsilon_s'(\lambda) \tag{6}$$

where $\varepsilon_k'(\lambda)$ is the first differential of the specific extinction coefficient of the *k*th chromophore with respect to wavelength and $\varepsilon_s'(\lambda)$ is the first differential of the scattering coefficient with respect to wavelength. We refer to the first and second term on the right of Eq. (6) as the absorption and scattering term but both terms have dependence on both absorption and scattering coefficient through the differential pathlength and differential scatterlength, respectively.

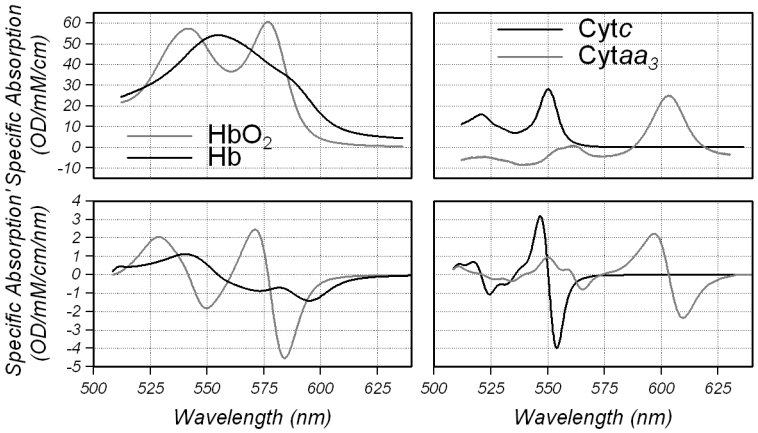

Fig. 1. Specific extinction spectra (upper) and 1st differential of the specific extinction spectra (lower) of HbO_2 and Hb (left) and Cytc and $Cytaa_3$ (right).

#169970 - $15.00 USD Received 6 Jun 2012; revised 19 Jul 2012; accepted 21 Jul 2012; published 25 Jul 2012

One advantage of using the first differential instead of the attenuation spectrum is that it makes the measurement, $A'(\lambda)$, approximately linear with respect to the absolute chromophore concentrations (see Eq. (6)). In addition, measurement of the scattering coefficient of tissue has been shown to be slowly varying function of wavelength compared to the chromophores [29] so that the scattering term of Eq. (6) is small compared to the absorption term. Finally, the first differential spectrum has preferential sensitivity to the cytochromes over the hemoglobin because the absorption spectra of the former are sharper than the latter. This is illustrated in Fig. 1 which compares the specific extinction spectra of HbO_2, Hb, Cyt*c* and $Cytaa_3$ and the first differential of the specific extinction spectra. The magnitude of the specific extinction spectra of Cyt*c* and $Cytaa_3$ is approximately half the magnitude of the specific extinction spectra of HbO_2 and Hb whereas the magnitude of the first differential of the extinction spectra of Cyt*c* and $Cytaa_3$ are approximately equal to that of HbO_2 and twice that of Hb.

2.3. Monte Carlo simulations

A Monte Carlo simulation of light transport through tissue was implemented in Delphi 2010 (Embarcadero, CA) as a Win32 application. The model follows multiple photons launched from the source fiber into a semi-infinite medium assuming zero absorption, a given anisotropy factor and a given full scattering coefficient. It generates a histogram, $\mathrm{H}(x,\mu_s)$, that represents the fraction of launched photons that were detected as a function of distance, *x,* that the photon traveled in the medium before being detected and for a given scattering coefficient. The scattering angle was calculated using the Henyey-Greenstein scattering function [30] and the anisotropy factor was set to 0.9 for all simulations. The model uses the radial symmetry to decrease the computational time. Photons are launched with equal probability over the area and acceptance cone of the source fiber and only photons which exit the medium within the acceptance cone of the detector fiber and in an annulus between the inter optode spacing plus and minus the detector fiber radius are detected. The detected photons are then weighted by the fraction of the circumference at the exit radius that falls within the detector fiber. The source and detector fiber acceptance cones are corrected for the refractive index of tissue (1.3). The code is multi-threaded to make full use of multi-core processors. The photons are followed until they exit the medium or for a maximum of 500mm at which point they would be extinguished by the absorption. It was found that the parameter most sensitive to the maximum pathlength was the differential pathlength when the absorption coefficient was zero. The value of 500mm was chosen because this value had negligible impact on this parameter.

For each simulation, 10^8 photons were launched and, depending on scattering coefficient, between 1.6 and 6.1 × 10^5 were detected based on statistics of between 0.3 and 1.2 × 10^6 photons that exited within the detection annulus.

Once the histogram has been generated for each scattering coefficient, the intensity of the detected light, I_D, can then be calculated for any given absorption coefficient of the tissue by

$$I_D = I_S \int_0^\infty \mathrm{H}(x,\mu_s) e^{-u_a x} dx \tag{7}$$

where I_S is the number of photons launched per second (source light intensity), x is the distance that the photons have traveled. The exponential factor gives the fraction of photons which are not absorbed by the medium. Using Eqs. (1) and (7), and the definition of the differential pathlength given in Eq. (3), the differential pathlength can be calculated from

$$\rho = \left(\frac{1}{I_D}\right) \int_0^\infty \mathrm{H}(x,\mu_s)\, x e^{-u_a x} dx \tag{8}$$

#169970 - $15.00 USD Received 6 Jun 2012; revised 19 Jul 2012; accepted 21 Jul 2012; published 25 Jul 2012

Equation (8) confirms that the differential pathlength is equal to the mean distance traveled [31] but there is no simple physical interpretation for the differential scatterlength. Using Eqs. (1) and (7), and the definition of the differential pathlength given in Eq. (3), the differential scatterlength can be calculated from

$$\sigma = -\left(\frac{1}{I_D}\right)\int_0^\infty \frac{\partial \mathrm{H}(x,\mu_s)}{\partial \mu_s} e^{-u_a x} dx \tag{9}$$

and the differential of the histogram can be calculated numerically from the difference between two histograms with slightly different scattering coefficients.

Whereas generating the histogram is computationally time consuming, Eqs. (7), (8) and (9) can be applied to rapidly calculate the attenuation, differential pathlength and differential scattering spectrum for a given absorption spectrum. The absorption coefficient is calculated at a particular wavelength from the chromophore concentrations using Eq. (2).

2.4. Spectral fitting

To calculate the concentration of Hb, HbO_2 and Cyt*c*, we first estimate the concentrations of each chromophore and use Eq. (2) to calculate μ_a and then Eq. (8) to calculate differential pathlength at every wavelength. We perform a least squares linear fit of the first differential of the attenuation spectrum to Eq. (6) to calculate the next iteration of the chromophore concentrations. The scatterlength has a very weak wavelength-dependence and this term can be fitted as an offset. In practice, the chromophore spectra are so orthogonal and the differential pathlength such a weak function of the absorption coefficient that this process converges very rapidly from any estimation of chromophore concentration. Total hemoglobin (HbT) is defined as the sum of HbO_2 and Hb and hemoglobin saturation (SO_2) is calculated from the ratio HbO_2 to HbT.

2.5. In vitro studies

Liquid phantoms were made from a mixture of fresh rat blood, intralipid and cytochrome c in physiological saline buffered by 20mM HEPES at pH 7.4. Fresh rat blood was obtained from the tail vein of Wistar rats and the hemoglobin content was measured with a co-oximeter (Rapidlab 845, Bayer Corporation Diagnostics Division, Norwood, MA) and converted to a concentration in units of μmoles/L assuming an atomic weight of hemoglobin to be 64,500g/mole. All blood samples had a combined met-hemoglobin and carbon monoxy-hemoglobin content of less than 2%. Bovine Cyt*c* was obtained from Sigma and used without further purification. Stock solutions of Cyt*c* were reduced with a small quantity of sodium ascorbate and the concentration of Cyt*c* was calculated from the absorption spectrum measured with a spectrophotometer using the same specific absorption spectrum as used in the subsequent studies.

The phantom was measured in a 6mL cylindrical chamber of inside diameter 17mm maintained at 37°C by a water jacket. The phantom was stirred with a glass stir bar and oxygen tension within the chamber was measured from the fluorescence lifetime of a phosphorescent membrane (Tautheta Instruments, Boulder, CO) located at the bottom of the chamber. The phantom was reversibly oxygenated or deoxygenated under computer control by exchange of oxygen across 90mm of silicone tubing (Renasil, Braintree Scientific, Braintree, MA) immersed in the cell suspension. Deoxygenation was aided by the addition of a small quantity of yeast to the phantom.

2.6. In vivo studies

All animal studies were carried out with approval of the local Institutional Animal Care and Use Committee. Wistar rats were anesthetized with 2% isoflurane, a tracheotomy performed and the animals mechanically ventilated. A catheter was sited in the femoral artery for collection of blood samples for blood gas analysis and for continuous monitoring of blood

#169970 - $15.00 USD Received 6 Jun 2012; revised 19 Jul 2012; accepted 21 Jul 2012; published 25 Jul 2012

pressure and heart rate. A second catheter was sited in the femoral vein for infusion of drugs where required. The fur over the head was shaved and the scalp removed. The skull over the parietal cortex was then thinned to translucency with a burr and the bone sealed with cyanoacrylate glue. Rectal temperature was monitored continuously and the animals maintained at 37°C using a heated water mattress. End-tidal CO_2 was monitored continuously with a capnogram and maintained so that arterial CO_2 tension was in the range 35-40mmHg. Arterial saturation was monitored continuously with a pulse oximeter. A computerized gas blender was used to mix the inspired gases and baseline inspired oxygen fraction (FiO_2) was set to 0.30 with the balance nitrogen. At the end of surgery, the isoflurane was decreased to 1.5% and the animals were allowed to stabilize for one hour before commencement of the study. Results are expressed as mean ± SD (n = 6).

3. Results

3.1. Simulations

Figure 2 compares the spectrum of the reduced scattering coefficient of 1% intralipid [32], the absorption spectrum of hemoglobin at a concentration of 60µmoles/L and a saturation of 75%, and the absorption spectrum of 10µmoles/L of reduced Cyt*c* in the wavelength range 510-640nm. The 1% intralipid models the scattering coefficient of the brain and the hemoglobin and Cyt*c* values approximate those found in the rat brain. The absorption spectrum is dominated by hemoglobin and the absorption of hemoglobin is almost one order of magnitude greater than the absorption of Cyt*c*. Figure 2 also illustrates that the absorption spectra are more feature rich than the scattering spectrum.

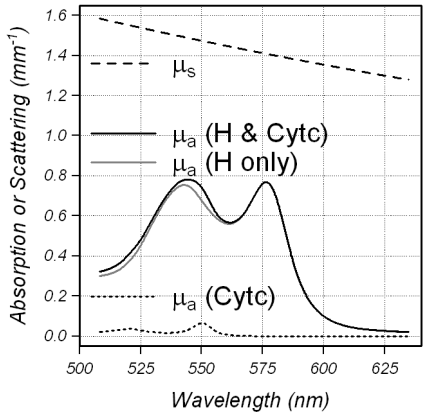

Fig. 2. Wavelength dependence of the scattering coefficient, absorption coefficients of 60µmoles/L hemoglobin (H) at a saturation of 75% with (H & Cyt*c*) and without (H only) 10µmoles/L of Cytc, and absorption coefficient of 10µmoles/L of Cytc.

The attenuation spectra, differential pathlength and differential scatterlength calculated with the Monte Carlo simulation using the optical properties shown in Fig. 2, are shown in Fig. 3. The scatterlength is negative, e.g. an increase in scattering coefficient creates a decrease in attenuation, and the scatter length is shown scaled by a factor of −1 for reasons of clarity. The absolute attenuation depends strongly on the exact numerical aperture and the coupling efficiency of the fibers, the latter can change between sample and reference. This results in an offset between the measured and modeled attenuation spectrum which complicates spectral fitting directly to the attenuation spectrum. This offset is removed by taking the first differential. The mean pathlength between 520 and 580nm is ≈2.16mm and varies by +12% at 520nm and –5% at 544nm. The differential pathlength increases substantially at longer wavelengths where the absorption due to hemoglobin is lower. The penetration of the light into the tissue is also expected to be deeper over this wavelength range.

#169970 - $15.00 USD Received 6 Jun 2012; revised 19 Jul 2012; accepted 21 Jul 2012; published 25 Jul 2012

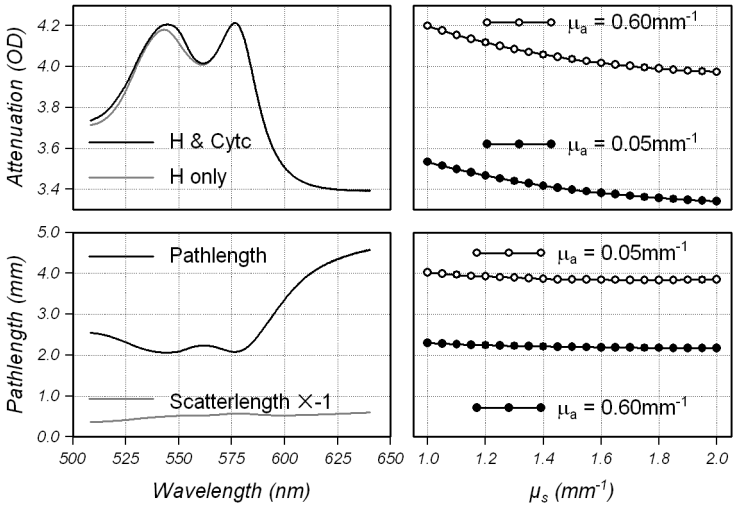

Fig. 3. Wavelength dependence and scattering dependence of attenuation, differential pathlength and differential scatterlength calculated from Monte Carlo simulations. Left Panels: Wavelength dependence of the attenuation (upper), differential pathlength and scatterlength (lower) for a media with the optical properties shown in Fig. 2. The differential scatterlength is scaled by a factor of −1 for clarity. Right panels: scattering dependence of attenuation (upper) and differential pathlength (lower) for a medium with absorption coefficients of 0.60 and 0.05mm^{-1}.

The variation of attenuation and differential pathlength with reduced scattering coefficient for absorption coefficients of 0.60 and 0.05mm^{-1} is shown in the right panels of Fig. 3. An absorption coefficient of 0.6mm^{-1} is representative of the absorption spectrum between 520 and 580nm whereas an absorption coefficient of 0.05mm^{-1} corresponds to a wavelength of ≈610nm close to the absorption peak of Cytaa$_3$. The attenuation is a strong function of reduced scattering coefficient at both absorption coefficients and varies by more than 25% of the dynamic range of the attenuation spectrum when the reduced scattering coefficient varies from 1.0 to 2.0mm^{-1}. In contrast, the differential pathlength is a weak function of reduced scattering coefficient and varies by less than 5% over the same range.

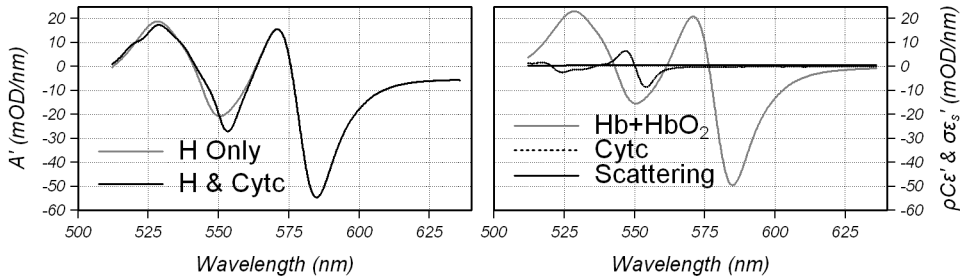

Fig. 4. First differential of the attenuation spectra with and without Cyt*c* from Fig. 3 (right) and decomposition into chromophore and scattering components (left).

Figure 4 shows the first differential of the attenuation spectra shown in Fig. 3 and the chromophore and scattering components that compose the first differential of the attenuation spectrum. The chromophore components are the product of the differential pathlength, chromophore concentration and first differential of the specific extinction spectrum and the scattering component is the product of differential scatter length and first differential of the scattering coefficient [see Eq. (6)]. The scattering component, which is ≈0.56mOD/nm, is much smaller than the absorption components mainly because the scattering coefficient is a

#169970 - $15.00 USD Received 6 Jun 2012; revised 19 Jul 2012; accepted 21 Jul 2012; published 25 Jul 2012

slowly varying function of wavelength but also because the magnitude of the differential scatterlength is approximately one fourth that of the differential pathlength.

3.2. Phantom studies

The ability to quantify and separate the hemoglobin and Cyt*c* chromophores was examined in phantoms by desaturating the hemoglobin in the absence or presence of reduced Cyt*c*. Representative data from the studies is shown in Fig. 5.

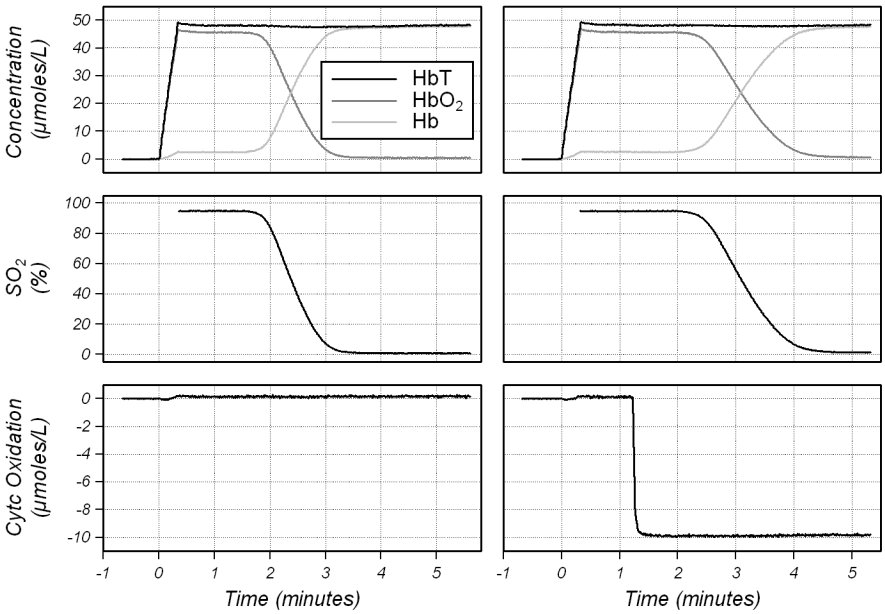

Fig. 5. Representative traces of hemoglobin concentration (upper panels) hemoglobin saturation (middle panels) and Cytc oxidation state (lower panels) of the phantom studies. Left panels. Initially, the phantom contained 1% intralipid and then 50µmoles/L of oxygenated hemoglobin was added at time zero followed by desaturation between 2 and 3 minutes. Right panels: Same as left except 10µmoles/L of reduced Cytc was added prior to desaturation.

The algorithm measures the concentration of reduced Cyt*c* because it has the sharp spectral feature at 550nm that is amplified by the first differential. The concentration of reduced Cyt*c* is plotted on a negative scale so that a reduction of Cyt*c*, that is, increased concentration of reduced Cyt*c* and a decrease concentration of oxidized Cyt*c* results in a downward deflection.

Initially, the phantom contained only 1% intralipid and the hemoglobin concentration was zero. At time zero, 50µmoles/L of hemoglobin was added to the oxygenated chamber resulting in a measured hemoglobin concentration of 48.5 ± 1.0µmoles/L and saturation of ≈94.8 ± 0.3% (mean ± SD, n = 8). Addition of hemoglobin in the absence of Cyt*c* resulted in a measured oxidation of Cyt*c* to +0.04 ± 0.01µmoles/L (n = 8). Subsequent addition of 10µmoles/L of reduced Cyt*c* resulted in a measured reduction of Cyt*c* to −10.1 ± 0.5µmoles/L (n = 4). The hemoglobin was then desaturated was passing nitrogen through the tubing immersed in the phantom resulting in a final concentration of 50.3 ± 2.1µmoles/L and a saturation of 1.7 ± 0.6% (n = 8). The change in the Cyt*c* signal on desaturation when 10µmoles/L of Cyt*c* was present or absent was −0.00 ± 0.1 (n = 4) and −0.1 ± 0.1µmoles/L (n = 4) respectively. The data shows that the algorithm can accurately measure the oxidation state of Cyt*c* in the presence of hemoglobin at any hemoglobin saturation.

The crosstalk between Cyt*c* and oxygenated or deoxygenated hemoglobin was quantified in greater detail by measuring the Cyt*c* signal when the phantom hemoglobin concentration was varied in the absence of Cyt*c* under oxygenated or deoxygenated conditions (Fig. 6). As

#169970 - $15.00 USD Received 6 Jun 2012; revised 19 Jul 2012; accepted 21 Jul 2012; published 25 Jul 2012

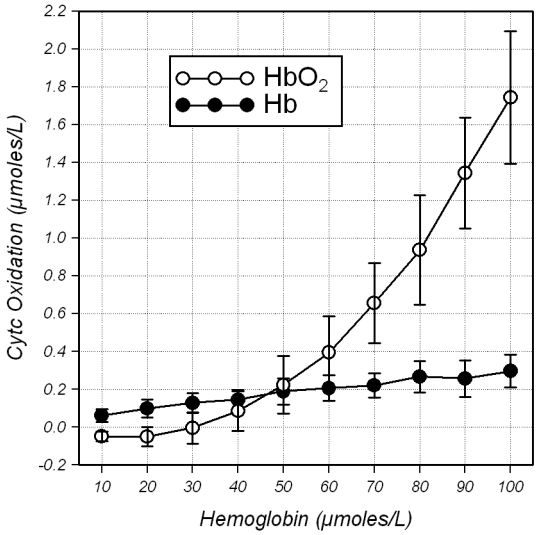

Fig. 6. Crosstalk between Cytc and hemoglobin as a function of oxygenated or deoxygenated hemoglobin concentration. 10 μmoles/L steps of hemoglobin were added to either a saturated or desaturated phantom contain 1% intralipid and no Cytc. Observed changes in Cytc were then attributed to crosstalk. Data is expressed as mean ± SD (n = 6).

could be expected, the crosstalk between HbO_2 and Cyt*c* was greater than between Hb and Cyt because the first differential of the HbO_2 is greater than that of Hb. The crosstalk from Hb into Cyt*c* was approximately linear with a value of 0.03 μmoles/L of Cyt*c* per μmoles/L of Hb. In contrast, the crosstalk of HbO_2 into Cyt*c* was nonlinear and reached 1.6μmoles/L (equivalent to 16% of Cyt*c* assuming a content of 10μmoles/L) at an HbO_2 concentration of 100μmoles/L. However, at physiological concentrations of hemoglobin (≈50-60μmoles/L) the crosstalk from HbO_2 and Hb is very similar and amounts to 2-4% of the total Cyt*c* content.

3.3. In vivo studies

The oxidation state of the hemes is independent of oxygen tension at high oxygen tension but it becomes progressively more reduced when oxygen tension limits oxidative phosphorylation and become fully reduced when the mitochondria become anoxic [7,33]. Unlike hemoglobin, the baseline oxidation state is not fully oxidized but depends on energetic status of the mitochondria [4]. A brief anoxia was performed in six rats weighing 250 ± 60g by switching the inspired oxygen fraction (FiO_2) to 0.00 for 45 seconds and then returning FiO_2 to 0.30. The anoxia is sufficiently long to nearly fully desaturate the brain but sufficiently short to allow the cerebral hemodynamics and metabolism to return to baseline in 5 minutes. It is believed that such a short period of anoxia will not result in tissue damage. The baseline physiological parameters were: mean arterial blood pressure 99 ± 14mmHg, heart rate 460 ± 20 beats/minute, temperature 37.0 ± 0.2°C, arterial pH 7.43 ± 0.03, arterial oxygen tension 136 ± 23mmHg and arterial CO_2 tension 38.2 ± 2.2mmHg.

Typical first differential spectra from the rat cortex under normoxic and anoxic conditions are shown in Fig. 7 along with the fit to the data, the residuals of the fit and the component of the fit attributed to Cyt*c*. The Cyt*c* component has been offset by 40mOD/nm for reasons of clarity. The residuals are the difference between the data and the fit and give an indication of the quality of the fit.

Figure 7 shows the time course of the hemoglobin concentration, mean hemoglobin saturation ($SmcO_2$) and reduced Cyt*c* concentration during the anoxia and recovery period. Baseline total hemoglobin was 56.2 ± 5.9μmoles/L, $SmcO_2$ was 67.7 ± 3.8% and Cyt*c* was 2.2 ± 0.3μmoles/L reduced. Anoxia led to a fall in $SmcO_2$ to 7.7 ± 1.9% and a reduction in Cyt*c* to −7.9 ± 0.9μmoles/L. The anoxia triggered a hyperemia as indicated by the increase in

#169970 - $15.00 USD Received 6 Jun 2012; revised 19 Jul 2012; accepted 21 Jul 2012; published 25 Jul 2012

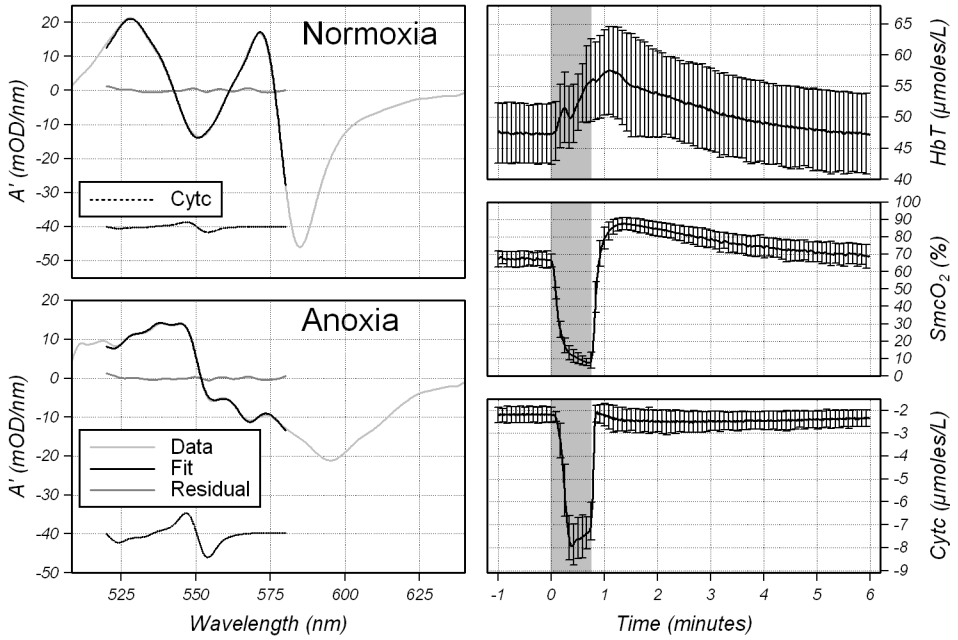

Fig. 7. Typical first-differential attenuation spectra, fitting model and time chromophore course during an anoxic challenge. Left panels: fitting residuals and Cytc component of the fit from the normoxic rat cortex (upper) and during anoxia (lower). The Cytc component has been offset by –40mOD/nm for reasons of clarity. Time course of the hemoglobin concentration (upper graph), mean hemoglobin saturation (middle graph) and Cytc during a brief anoxic insult and recovery. The shaded regions correspond to the period of anoxia. Data is expressed as mean ± SD (n = 6) and only every 10th error bar is shown for reasons of clarity.

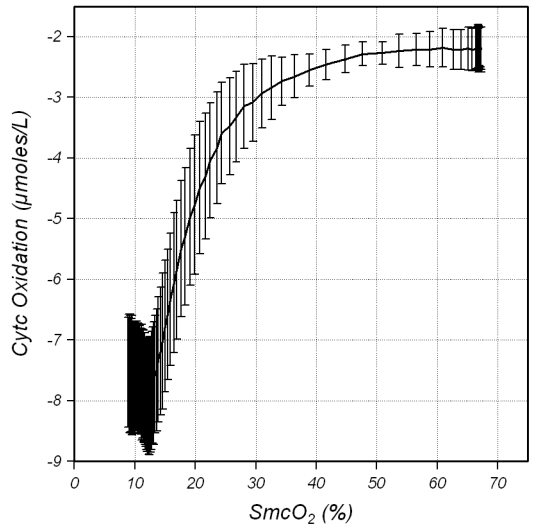

Fig. 8. Relationship between Cyt*c* oxidation and $SmcO_2$ during the onset of anoxia. Data is expressed as mean ± SD (n = 6). The x error bars are not shown for clarity.

HbT and, on reoxygenation, $SmcO_2$ increased to 87.7 ± 3.8% and Cyt*c* rapidly reoxidized to baseline followed by a very small but prolonged reduction below baseline. The RMS noise on

#169970 - $15.00 USD Received 6 Jun 2012; revised 19 Jul 2012; accepted 21 Jul 2012; published 25 Jul 2012

the baseline Cyt*c* signal is ≈0.035μmoles/L with 0.5 second time resolution equivalent to a 0.45% oxidation change in Cyt*c*.

Previous NIR work in the piglet [27] and the rat [34] has shown that the oxidation state of the Cu_A center is independent of hemoglobin saturation at normoxia and does not begin to reduce until there is a substantial decrease in $SmcO_2$. Figure 8 shows the relationship between Cyt*c* and $SmcO_2$ on the onset of anoxia for the data from Fig. 7 and is comparable with the piglet data where the Cu_A was independent of $SmcO_2$ until $SmcO_2$ fell below 50% [27]. Previously, Cu_A did not reduce until $SmcO_2$ fell below ≈30% in the rat [34] and the difference could due to the increased crosstalk in the NIRS rat studies, as evidenced by the small oxidation prior to reduction, or could be a strain difference; we find the baseline $SmcO_2$ is typically 65% in Wistar rats and 75% in Sprague Dawley rats under the same ventilation conditions.

4. Discussion

The primary goal of tissue spectroscopy is to accurately quantify the tissue chromophore concentrations. Accurately separating the chromophore concentrations is an important part of this goal which becomes critical when one chromophore is at a much lower concentration than another or has a much weaker extinction spectrum. This problem is compounded when trying to measure the mitochondrial signals in the rat brain because the cytochromes are both at a lower concentration and have weaker absorption spectra. The studies presented here show that Cyt*c* can be successfully separated from hemoglobin and this is in large part due to taking the first differential of the attenuation spectrum. The first differential provides preferential sensitivity to the mitochondrial signals over the hemoglobin signals because they have sharper specific absorption spectrum and, furthermore, the first differential of the chromophore spectra are highly orthogonal which makes the inversion matrix well-conditioned allowing their precise separation. The non-linearity between the attenuation and absorption leads to a distortion of the attenuation spectrum with regard to the absorption spectrum which must be precisely accounted for by the light-transport model in order in order to prevent crosstalk into Cyt*c*. For the first differential fitting, the first differential of the attenuation spectrum is still distorted with respect to the first differential of the absorption spectrum but, in this case, the distortion is given by the wavelength-dependence of the differential pathlength. We find that the hemoglobin and Cyt*c* traces are very similar when fitting the first differential of *in vivo* data with a simple linear model that assumes both the differential pathlength and differential scattering are wavelength independent compared to using the full Monte Carlo model. Thus the main role of the Monte Carlo model is to accurately scale the calculated chromophore concentrations rather than to correct for the spectral distortions and provide precise separation.

The first differential of the attenuation spectrum is only weakly dependent on the reduced scattering coefficient through the differential pathlength and the scattering term. We are not able to calculate the scattering coefficient from the attenuation spectra and instead have to assume a value. This may seem to be a weakness of the algorithm but, in terms of separating the hemoglobin and cytochrome signals, it is in fact a strength because it means that errors in the estimation of the scattering coefficient do not lead to crosstalk between the hemoglobin and cytochrome signals. Furthermore, changes in the scattering coefficient during a study will also not lead to cross talk. Overall, the weak dependence of the parameters on the model of light transport through the tissue makes the algorithm robust to the inevitable errors in the model and prevents the model-data mismatches propagating from into chromophore concentration errors.

Intensity calibration is also relatively simple with the first differential algorithm because the optical properties of the intensity phantom do not need to be known as long as the absolute attenuation spectrum is not more than linear with wavelength. The first differential removes any offset on the attenuation spectrum due to wavelength-independent coupling losses between the fiber and the tissue and any other wavelength independent effects. Furthermore the offset used to fit the scattering term automatically corrects for a linear term in the

#169970 - $15.00 USD Received 6 Jun 2012; revised 19 Jul 2012; accepted 21 Jul 2012; published 25 Jul 2012

attenuation of the reference phantom allowing Teflon, a fluorocarbon with negligible absorption at visible wavelengths but high scattering coefficient, to be used as the attenuation reference.

One weakness of the differential algorithm is that it requires attenuation spectra with high spectral resolution, high signal to noise and negligible fixed-pattern noise. The spectral resolution and signal to noise can easily be obtained with 0.3m spectrographs and cooled 2-dimension CCD detectors. Cooling to 210 Kelvin essentially removes the thermally induced signal, even for hot pixels, preventing thermal fixed-pattern noise. The integration of charge over a column of pixels on a 2-dimensional CCD also averages pixel to pixel variations in quantum efficiency and so minimizes fixed-pattern noise. Sufficient light was obtained from a filtered 100W tungsten halogen lamp but this could be replaced with a high-power white light emitting diode (LED) reducing overall system cost and increasing portability.

It was found that crosstalk into Cyt*c* was greater from HbO_2 compared to Hb (Fig. 6) as might be anticipated because HbO_2 has a more intense first-differential spectrum. However, the crosstalk is not linear with HbO_2 as might be expected but increases substantially at high HbO_2 concentrations. This may limit the utility of the technique in certain tissues with a very high hemoglobin content but the crosstalk at the concentrations of hemoglobin found in the rat brain (50-60μmoles/L) represents only 2-4% of the total Cyt*c* content making it suitable for brain studies. The crosstalk with HbO_2 may be a result of the corpuscular nature of red blood cells. As is common, the hemoglobin concentration is modeled as homogeneous background at a concentration of 50-60μmoles/L whereas, in reality, it is packed into red blood cells at a concentration of 5-6mmoles/L and the red blood cells make up ≈1%V/V. The crosstalk may be reduced by taking the heterogeneity into account, either analytically at the level of the spectra as has been attempted before [35], or directly in the Monte Carlo simulation.

Cyt*c* usually resides in the mitochondria inner membrane space where it transfers electrons from the bc_1 complex to CytOx as part of the electron transport chain. These electrons are subsequently used to reduce oxygen to water. Cyt*c* does not react directly with oxygen and, unlike hemoglobin, Cyt*c* is not fully oxidized at high oxygen tension. The oxidation state of Cyt*c* is independent of oxygen tension at high oxygen tension but Cyt*c* does become progressively reduced when oxygen tension falls to low levels sufficient to limit CytOx. Our previous work in piglet brain with the Cu_A center of CytOx predicts, and is confirmed here, that the oxidation state of Cyt*c* will be independent of oxygen tension at normoxia and only become reduced under hypoxic conditions [27,36]. This makes Cyt*c* a sensitive indicator of hypoxia at the mitochondrial level making it useful for functional activation studies, where there is considerable controversy as to mitochondrial oxygenation, and to ischemic studies where hypoxia at the mitochondrial level is the primary cause of the loss in tissue viability.

Another major role of Cyt*c* it to trigger programmed cell death when it is released from the mitochondria into the cytosol (see [37] for a review). Our previous work in cell culture shows that Cyt*c* becomes reduced when released into cytosol and this reduction allows Cyt*c* to be used as a sensitive and quantitative measure of Cyt*c* release [38]. Implementation of this algorithm and measurement of Cyt*c* oxidation states should be unique physiological information in the study of ischemia and seizures, both of which can lead to the loss of tissue viability.

Acknowledgments

This work was funded by the National Institute of Neurological Disorders and Stroke (NINDS), grant NIH R01NS054298.

#169970 - $15.00 USD Received 6 Jun 2012; revised 19 Jul 2012; accepted 21 Jul 2012; published 25 Jul 2012